universe

IMPACT FACTOR 2.5

CITESCORE 4.3

Article

The Intrinsic Correlations between Prompt Emission and X-ray Flares of Gamma-Ray Bursts

Xing-Ting Zhong, Si-Yuan Zhu, Li-Ming Zhuo, Zeng Zhang and Fu-Wen Zhang

MDPI

https://doi.org/10.3390/universe10090343

universe

MDPI

Article

The Intrinsic Correlations between Prompt Emission and X-ray Flares of Gamma-Ray Bursts

Xing-Ting Zhong [1], Si-Yuan Zhu [1,2,*], Li-Ming Zhuo [1], Zeng Zhang [1] and Fu-Wen Zhang [1,3,*]

[1] College of Physics and Electronic Information Engineering, Guilin University of Technology, Guilin 541004, China; 1026kk@163.com (X.-T.Z.); wqpepmm676@163.com (L.-M.Z.); zhangzeng0304@163.com (Z.Z.)
[2] School of Physics and Astronomy, Sun Yat-sen University, Zhuhai 519082, China
[3] Key Laboratory of Low-Dimensional Structural Physics and Application, Education Department of Guangxi Zhuang Autonomous Region, Guilin 541004, China
* Correspondence: glzhusiyuan@163.com (S.-Y.Z.); fwzhang@pmo.ac.cn (F.-W.Z.)

Abstract: X-ray flare (XRF) is a common phenomenon in the X-ray afterglow of gamma-ray bursts (GRBs). Although it is commonly believed that XRFs may share a common origin with prompt emission, i.e., the "internal" origin, the origin of XRFs is still unknown. In this work, we compile a GRB sample containing 31 GRBs with a single XRF, a well-measured spectrum, and a redshift, and investigate the intrinsic properties and correlations between prompt emission and the XRFs of these events. We find that the distributions of main physical parameters of prompt emission and XRFs are basically log-normal. The median value of the rise time is shorter than the decay time for all flares, with a ratio of about 1:2, which is similar to the fast rise and exponential decay structure of prompt emission pulses. We also find that the prompt emission energy ($E_{\rm iso}$) and peak luminosity ($L_{\rm iso}$) have tight correlations with XRF energy ($E_{\rm X,iso}$) and peak luminosity ($L_{\rm X,p}$), $E_{\rm iso} \propto E_{\rm X,iso}^{0.74}$ ($L_{\rm X,p}^{0.62}$) and $L_{\rm iso} \propto E_{\rm X,iso}^{0.85}$ ($L_{\rm X,p}^{0.68}$). However, the durations of prompt emissions are independent of the temporal properties of XRFs. Furthermore, we also analyze the three-parameter correlations between prompt emissions and XRFs, and find that there are tight correlations among the XRF peak time ($T_{\rm p,z}$), $L_{\rm X,p}$, and $E_{\rm iso}/L_{\rm iso}$, $L_{\rm X,p} \propto T_{\rm p,z}^{-1.08} E_{\rm iso}^{0.84}$ and $L_{\rm X,p} \propto T_{\rm p,z}^{-1.09} L_{\rm iso}^{0.71}$. Interestingly, these results are very similar to the properties of an X-ray plateau in GRBs, which indicates that X-ray flares and plateaus may have the same physical origin, and strongly supports that the two emission components originate from the late-time activity of the central engine.

Keywords: gamma-ray burst; general methods; data analysis

Citation: Zhong, X.-T.; Zhu, S.-Y.; Zhuo, L.-M.; Zhang, Z.; Zhang, F.-W. The Intrinsic Correlations between Prompt Emission and X-ray Flares of Gamma-Ray Bursts. *Universe* **2024**, *10*, 343. https://doi.org/10.3390/universe10090343

Academic Editor: Patrizia Romano

Received: 24 July 2024
Revised: 19 August 2024
Accepted: 21 August 2024
Published: 27 August 2024

1. Introduction

Gamma-ray bursts (GRBs) are the most extreme electromagnetic emission phenomenon in the universe. According to the bimodal distribution with a boundary at $T_{90} \sim 2$ s, GRBs can be classified as long-duration GRBs (LGRBs, $T_{90} > 2$ s) and short-duration GRBs (SGRBs, $T_{90} < 2$ s), where T_{90} is the time during which the cumulative counts of photons in a specified energy range increase from 5% to 95% of all such photons that are recorded in the burst [1]. It is widely believed that LGRBs originate from the massive collapsars and SGRBs originate from the compact binary mergers [2–4]. A central engine driving the relativistic jet will exist after the explosion, though it is uncertain whether that is a black hole or a magnetar [5].

After the successful launch of Swift in 2004 [6], several special features were discovered in the X-ray afterglows of GRBs, especially X-ray flares (XRFs). They present generally a sharp rise followed by sharp decay features [7]. XRFs are common phenomena in the X-ray afterglows of GRBs and have been observed in both LGRBs and SGRBs [8–12]. Previous studies found that the XRFs of SGRBs present similar properties to those of LGRBs, which suggests that XRFs may share a common origin in both LGRBs and SGRBs [11,13]. The

number of XRFs in one GRB is indeterminate. The vast majority of XRFs occur before 10^3 s (early XRFs), while a few XRFs occur after 10^6 s (late XRFs) [14,15].

Although XRFs occur in the afterglow phase, the external shock origin is unsupported by their temporal and spectral properties. According to the external forward shock models, a power-law decay afterglow is expected, which is clearly inconsistent with the shape features of XRFs [7,16]. Moreover, the shapes of XRFs can be produced by reverse shocks. However, reverse shocks cannot explain multiple XRFs in a single GRBs and contribute mainly in the ultraviolet and optical bands [17]. Due to the lack of ultraviolet or optical flares simultaneously accompanying XRFs, the reverse shock model is tentatively ruled out [7]. In addition, the observed large $\triangle F/\mathrm{F}$ values cannot be produced by reverse shock, unless there is an extremely balanced condition [17,18].

Refreshed shock is a possible origin of XRFs [19,20]. However, the small $\triangle T/T_{\mathrm{p}} = 0.13$ is not favourable for the refreshed shock model [18,20]. In addition, the fluxes before and after XRF approximately lie on the same power-law decay, which suggests that XRFs originate from a different physical component than that responsible for the underlying power-law decay, and almost rules out the external shock model [7,10,20,21]. Furthermore, It is suggested by the spectral analyses that XRFs are different from the underlying power-law component that is the external origin and have a hard-to-soft evolution pattern, which is similar to prompt emission [22–25].

Although the refresh shock model cannot be completely ruled out, most XRFs can be explained more naturally by a long active central engine [18,24]. It is revealed that the temporal and spectral properties of XRFs are analogous to those of their prompt emission. Ref. [26] analyzed the spectral lag (τ) of XRFs and found $L_{\mathrm{iso}} \propto \tau^{-0.95}$, which is the same with the prompt pulses, and present evidence that prompt pulses and flares are produced by the same physical process. Furthermore, several temporal analyzes of XRFs, such as variability and spectral lag, support that the XRFs and the prompt emission of GRBs share a common origin. [15,27,28]. Ref. [29] analyzed the spectra of XRFs and derived the Γ_0–L_{iso} relation through a thermal component that may originate from photospheric emission, which is consistent with the result of the prompt emission. In addition, previous studies have found some correlations between XRFs and prompt emission within a burst [30–33]. Recently, Ref. [12] investigated the distributions of XRFs and solar flares, and found that there exists similar power-law distributions of XRFs and solar flares. This can be well explained by a fractal-diffusive, self-organized criticality model. Both types of flares may be driven by a magnetic reconnection process [12,34].

Since redshift measurements of GRBs are difficult, the previous studies of XRFs were mainly performed in the observer frame. The analysis of the properties of XRFs in the rest frame and the relationships between XRFs and prompt emission can reflect the intrinsic physics of XRFs and GRBs. In addition, Ref. [32] preliminarily found that the plateau phase energy and flare energy have similar correlations with the prompt emission energy. In this paper, we focus on the GRBs with flares and well-measured redshift to investigate the statistical characteristics of the prompt emissions and XRFs in the rest frame and further explore the relations between XRFs and prompt emission. This paper is organized as follows. In Section 2, we describe sample selection and data analysis. In Section 3, we analyze the statistical properties and correlations between prompt emission and XRFs. The summary and discussion are shown in Section 4. The cosmological constants in this paper are $H_0 = 71$ km s^{-1} Mpc^{-1}, $\Omega_{\mathrm{M}} = 0.27$, and $\Omega_\Lambda = 0.73$. The symbolic notation of $Q_{\mathrm{n}} = Q/10^{\mathrm{n}}$ is adopted.

2. Data and Method

In order to investigate the relationship between the prompt emission and the XRFs of GRBs in the rest frame, we need a GRB sample with an XRF, a redshift (z), and well-constrained spectral parameters. Ref. [13] selected all GRBs with XRFs observed from the Swift/XRT for the last 15 years (up to April 2021). They fitted the X-ray lightcurve (0.3–10 KeV) after considering the various components of the afterglow and obtained the

parameters of XRFs. The XRF data are available in Ref. [13]. For more details on data selection and fitting, please refer to Ref. [13]. The main physical parameters of XRFs in the rest frame include the duration defined as full width at half maxima ($T_{\rm FWHM,z}$), the peak time ($T_{\rm p,z}$), the rise time ($T_{\rm r,z}$), the decay time ($T_{\rm d,z}$), the isotropic energy ($E_{\rm X,iso}$), and the isotropic luminosity at the peak ($L_{\rm X,p}$), which are shown in Table 1. The prompt emission data are adopted from the Fermi catalog[1] and the General Coordinates Network (GCN)[2]. We select the GRBs with well-constrained peak energy ($E_{\rm p}$) in the νf_ν spectrum. Finally, we compile a sample of 31 GRBs (30 LGRBs and 1 SGRB) with XRFs. Note that the GRBs in our sample all have a single XRF.

We derive the rest frame parameters of prompt emission. In this paper, both the isotropic energy ($E_{\rm iso}$) and the isotropic peak luminosity ($L_{\rm iso}$) are corrected to the rest frame energy band of 1–10^4 keV. The $E_{\rm iso}$ is calculated by

$$E_{\rm iso} = \frac{4\pi D_{\rm L}^2 S_\gamma k}{(1+z)}, \tag{1}$$

where $D_{\rm L}$ is the luminosity distance, S_γ is the time integral fluence, and k is the k-correction factor. The k is defined as

$$k = \frac{\int_{1/(1+z)}^{10^4/(1+z)} EN(E)dE}{\int_{e_{\rm min}}^{e_{\rm max}} EN(E)dE}, \tag{2}$$

where $e_{\rm min}$ and $e_{\rm max}$ are the observational energy band of fluence, $N(E)$ denotes the photon spectrum of GRBs [35]. In our sample, $N(E)$ are fitted by Band model or cutoff power law (CPL) model [36]. The $L_{\rm iso}$ is estimated by

$$L_{\rm iso} = 4\pi D_{\rm L}^2 F_{\rm p} k, \tag{3}$$

where $F_{\rm p}$ is the peak flux. The rest frame duration ($T_{90,\rm z}$) and peak energy ($E_{\rm p,z}$) can be derived by $T_{90,\rm z} = T_{90}/(1+z)$, and $E_{\rm p,z} = E_{\rm p}(1+z)$. These prompt emission parameters are also listed in Table 1.

In order to quantitatively investigate the correlation between prompt emission and XRFs, we adopt the method presented in [37] to obtain the best-fit coefficients. The analysis method of three-parameter correlation is presented. We assume the three-parameter linear model,

$$\log y = a + b\log x_1 + c\log x_2, \tag{4}$$

where a is constant, b and c are the coefficients of x_1 and x_2, respectively. Due to the complexity of GRB sampling, an intrinsic scattering parameter ($\sigma_{\rm int}$) is introduced, as has usually been done by other researchers [38,39]. This extra variable follows a normal distribution of $\mathrm{N}(0, \sigma_{\rm int}^2)$, which represents all the contributions to y from other unknown hidden variables. The joint likelihood function for the coefficients of a, b, c, and $\sigma_{\rm int}$ is

$$\begin{aligned}\mathcal{L}(a,b,c,\sigma_{\rm int}) \propto & \prod_i \frac{1}{\sqrt{\sigma_{\rm int}^2 + \sigma_{y_i}^2 + b^2\sigma_{x_{1,i}}^2 + c^2\sigma_{x_{2,i}}^2}} \\ & \times \exp\left[-\frac{(y_i - a - bx_{1,i} - cx_{x,i})^2}{2(\sigma_{\rm int}^2 + \sigma_{y_i}^2 + b^2\sigma_{x_{1,i}}^2 + c^2\sigma_{x_{2,i}}^2)}\right],\end{aligned} \tag{5}$$

where i is the corresponding serial number of GRBs in our sample. Our linear model and likelihood function can also be conveniently applied to the two-parameter correlation by simply taking $c = 0$.

We use a python module *emcee*[3] to obtain the best-fit coefficients, which is based on the Markov chain Monte Carlo (MCMC) method. The *emcee* can obtain the best-fit values and their uncertainties of parameters a, b, c, and $\sigma_{\rm int}$ by generating sample points of the probability distribution [40]. For each Markov chain, we generate 10^6 sample points according to the likelihood function.

Table 1. The parameters of both prompt emission and XRFs of GRBs in the rest frame.

GRB	$T_{90,z}$ (s)	$E_{p,z}$ (keV)	$E_{iso,52}$ (erg)	$L_{iso,52}$ (erg/s)	$T_{FWHM,z}$ (s)	$T_{p,z}$ (s)	$T_{r,z}$ (s)	$T_{d,z}$ (s)	$L_{X,p,49}$ (erg/s)	$E_{X,iso,50}$ (erg)
050908	4.47 ± 0.45	291.18 ± 29.12	4.02 ± 0.39	1.48 ± 0.21	10.26 ± 1.03	89.22 ± 0.20	1.02 ± 0.10	9.24 ± 0.92	2.07 ± 0.30	1.56 ± 0.22
060115	30.82 ± 3.08	280.86 ± 45.30	6.74 ± 0.75	1.01 ± 0.11	20.67 ± 2.07	90.38 ± 3.53	9.33 ± 0.93	11.34 ± 1.13	1.66 ± 0.26	2.64 ± 0.39
060204B	41.75 ± 4.15	323.24 ± 136.91	5.76 ± 0.38	0.64 ± 0.10	9.21 ± 0.92	95.34 ± 0.42	2.76 ± 0.28	6.45 ± 0.65	4.11 ± 0.27	2.88 ± 0.14
060418	41.42 ± 4.14	572.47 ± 57.25	11.99 ± 1.20	1.86 ± 0.11	5.90 ± 0.59	51.85 ± 0.12	1.32 ± 0.13	4.58 ± 0.46	29.50 ± 1.07	13.10 ± 0.40
060707	14.96 ± 1.50	292.05 ± 44.25	5.49 ± 0.65	1.09 ± 0.20	5.47 ± 0.547	42.20 ± 0.14	0.22 ± 0.02	5.25 ± 0.53	2.30 ± 0.63	0.91 ± 0.24
060719	26.42 ± 2.64	138.96 ± 13.90	1.38 ± 0.09	0.34 ± 0.03	12.89 ± 1.29	81.54 ± 4.18	5.33 ± 0.53	7.56 ± 0.76	0.17 ± 0.04	0.17 ± 0.04
060814	49.71 ± 4.97	751.19 ± 169.53	31.58 ± 9.27	7.31 ± 1.89	13.30 ± 1.33	44.40 ± 0.40	1.55 ± 0.16	11.74 ± 1.17	15.40 ± 0.79	15.00 ± 0.52
070318	40.63 ± 4.06	360.20 ± 35.99	0.99 ± 0.04	0.09 ± 0.01	50.87 ± 5.09	154.93 ± 2.51	19.78 ± 1.98	31.09 ± 3.11	0.26 ± 0.01	1.01 ± 0.04
080210	12.36 ± 1.24	329.44 ± 32.94	7.46 ± 0.41	1.56 ± 0.20	5.95 ± 0.60	52.47 ± 0.55	2.35 ± 0.24	3.61 ± 0.36	9.74 ± 0.10	4.46 ± 0.40
081008	62.49 ± 6.25	261.23 ± 26.12	9.53 ± 0.44	0.56 ± 0.04	10.40 ± 1.04	100.22 ± 0.25	2.48 ± 0.25	7.92 ± 0.79	6.84 ± 0.28	5.37 ± 0.17
091029	10.45 ± 1.05	230.37 ± 65.66	7.59 ± 0.32	1.37 ± 0.08	18.49 ± 1.85	82.82 ± 3.40	6.33 ± 0.63	12.16 ± 1.22	0.57 ± 0.14	0.80 ± 0.16
101219B	21.94 ± 2.19	128.03 ± 7.15	0.17 ± 0.01	0.02 ± 0.00	75.08 ± 7.51	229.84 ± 7.44	31.78 ± 3.18	43.30 ± 4.33	0.03 ± 0.01	0.18 ± 0.01
111107A	6.83 ± 0.68	1026.76 ± 299.15	3.94 ± 0.58	2.11 ± 0.37	24.64 ± 2.46	83.25 ± 4.75	13.37 ± 1.34	11.27 ± 1.13	0.64 ± 0.14	1.23 ± 0.24
131030A	17.91 ± 1.79	406.22 ± 22.95	30.14 ± 1.83	10.48 ± 1.05	31.96 ± 3.20	49.97 ± 0.61	20.82 ± 2.08	11.14 ± 1.11	65.90 ± 2.43	164.00 ± 4.93
131117A	2.18 ± 0.22	221.85 ± 37.31	1.02 ± 0.16	0.85 ± 0.12	2.460 ± 0.25	18.86 ± 0.18	0.88 ± 0.09	1.58 ± 0.16	19.0 ± 1.67	3.70 ± 0.26
140419A	19.11 ± 1.91	1452.11 ± 416.30	148.26 ± 48.57	59.54 ± 24.07	5.62 ± 0.56	39.64 ± 0.33	1.61 ± 0.16	4.01 ± 0.40	21.30 ± 1.91	9.10 ± 0.61
140515A	3.20 ± 0.32	375.52 ± 107.60	5.42 ± 0.55	3.79 ± 0.42	356.23 ± 35.62	406.37 ± 2.80	104.06 ± 10.41	252.17 ± 25.22	1.04 ± 0.11	28.00 ± 2.87
140907A	35.84 ± 3.58	303.21 ± 17.25	2.57 ± 0.09	0.33 ± 0.02	28.57 ± 2.86	81.12 ± 4.58	6.38 ± 0.64	22.19 ± 2.22	0.14 ± 0.04	0.29 ± 0.07
141221A	15.05 ± 1.51	446.44 ± 78.39	1.71 ± 0.16	0.80 ± 0.05	53.36 ± 5.34	138.96 ± 6.71	24.50 ± 2.45	28.86 ± 2.89	0.69 ± 0.08	2.83 ± 0.31
150206A	26.95 ± 2.70	703.84 ± 108.05	51.87 ± 6.01	22.98 ± 5.16	159.11 ± 15.91	754.59 ± 3.43	94.87 ± 9.49	64.24 ± 6.42	18.90 ± 0.45	232.00 ± 4.38
151111A	17.10 ± 1.71	533.24 ± 43.43	5.37 ± 0.35	1.32 ± 0.26	11.08 ± 1.11	29.47 ± 0.93	4.83 ± 0.48	6.25 ± 0.63	10.70 ± 0.75	9.18 ± 0.67
160804A	83.06 ± 8.31	131.68 ± 4.88	2.03 ± 0.05	0.07 ± 0.01	21.80 ± 2.18	243.15 ± 0.97	6.06 ± 0.61	15.74 ± 1.57	0.48 ± 0.03	0.72 ± 0.40
161117A	49.31 ± 4.93	216.76 ± 4.39	20.83 ± 0.27	1.29 ± 0.05	9.86 ± 0.99	45.89 ± 0.22	4.36 ± 0.44	5.49 ± 0.55	83.30 ± 2.06	63.40 ± 1.51
161219B	6.05 ± 0.61	71.03 ± 19.28	0.01 ± 0.00	0.003 ± 0.00	86.26 ± 8.63	333.94 ± 2.57	24.33 ± 2.43	61.93 ± 6.19	0.01 ± 0.00	0.04 ± 0.00
170405A	36.52 ± 3.65	1204.23 ± 41.89	253.07 ± 2.55	39.11 ± 0.84	5.46 ± 0.55	35.77 ± 0.23	1.89 ± 0.19	3.57 ± 0.36	68.50 ± 3.65	28.60 ± 1.23
170705A	72.19 ± 7.22	294.61 ± 23.01	17.84 ± 0.54	7.96 ± 0.18	21.56 ± 2.16	65.65 ± 0.29	8.37 ± 0.84	13.18 ± 1.32	22.60 ± 0.38	37.40 ± 0.59
180325A	28.97 ± 2.90	993.89 ± 126.67	21.83 ± 3.45	30.60 ± 4.85	4.08 ± 0.41	24.89 ± 0.23	1.01 ± 0.10	3.07 ± 0.31	73.70 ± 4.69	22.70 ± 1.19
180620B	93.88 ± 9.39	371.90 ± 105.43	8.17 ± 0.22	1.28 ± 0.11	8.88 ± 0.89	48.02 ± 0.55	1.64 ± 0.16	7.24 ± 0.72	5.20 ± 0.56	3.44 ± 0.26
191221B	22.35 ± 2.24	809.80 ± 62.29	30.20 ± 3.02	12.33 ± 1.30	224.02 ± 22.40	447.20 ± 11.49	73.92 ± 7.39	150.10 ± 15.01	0.23 ± 0.01	3.98 ± 0.16
210411C	3.346 ± 0.34	56.62 ± 41.32	6.27 ± 0.52	4.53 ± 0.28	13.55 ± 1.36	45.52 ± 0.94	4.58 ± 0.46	8.97 ± 0.90	5.32 ± 0.42	5.50 ± 0.35
160410A	0.58 ± 0.05	3847.27 ± 967.25	8.49 ± 2.12	53.82 ± 7.69	17.54 ± 1.75	114.84 ± 7.13	8.90 ± 0.90	8.54 ± 0.854	0.17 ± 0.05	0.22 ± 0.07

3. Statistical Analysis

3.1. Parameter Distributions

The parameter distributions of both prompt emission and XRFs in our sample are analyzed and presented in Figure 1. We find that these parameters are basically log-normal distributions. To give a quantitative result, we make a Gaussian fitting for LGRBs, and the median values and dispersions of the distributions are listed in Table 2. The median values of the prompt emission duration and flare duration are similar. The median value of flare rise time is shorter than that of the decay time, with a ratio of about 1:2. This structure is similar to the FRED (fast rise and exponential decay) structure of prompt emission pulses [41]. The isotropic energy and peak luminosity distributions for both prompt emission and flares all span a wide range. $E_{\rm iso}$ are mainly distributed in the order range of 10^{50}∼10^{55}, while $E_{\rm X,iso}$ are mainly distributed in the order range of 10^{48}∼10^{52}, which is 2–3 orders less than the prompt emission. The larger dispersions may be due to the intrinsic properties of different center engines, such as the jet open angle, or other factors.

Table 2. The Best-fit Parameters of Distributions.

Parameter	Median Value	Dispersion
$T_{90,z}$	20.35 s	0.43
$E_{\rm p,z}$	344.61 keV	0.33
$E_{\rm iso}$	6.11×10^{52} erg	0.82
$L_{\rm iso}$	1.45×10^{52} erg s^{-1}	0.93
$T_{\rm FWHM,z}$	18.58 s	0.52
$T_{\rm p,z}$	84.49 s	0.39
$T_{\rm r,z}$	5.57 s	0.64
$T_{\rm d,z}$	12.04 s	0.49
$E_{\rm X,iso}$	4.02×10^{50} erg	0.86
$L_{\rm X,p}$	2.84×10^{49} erg s^{-1}	1.04

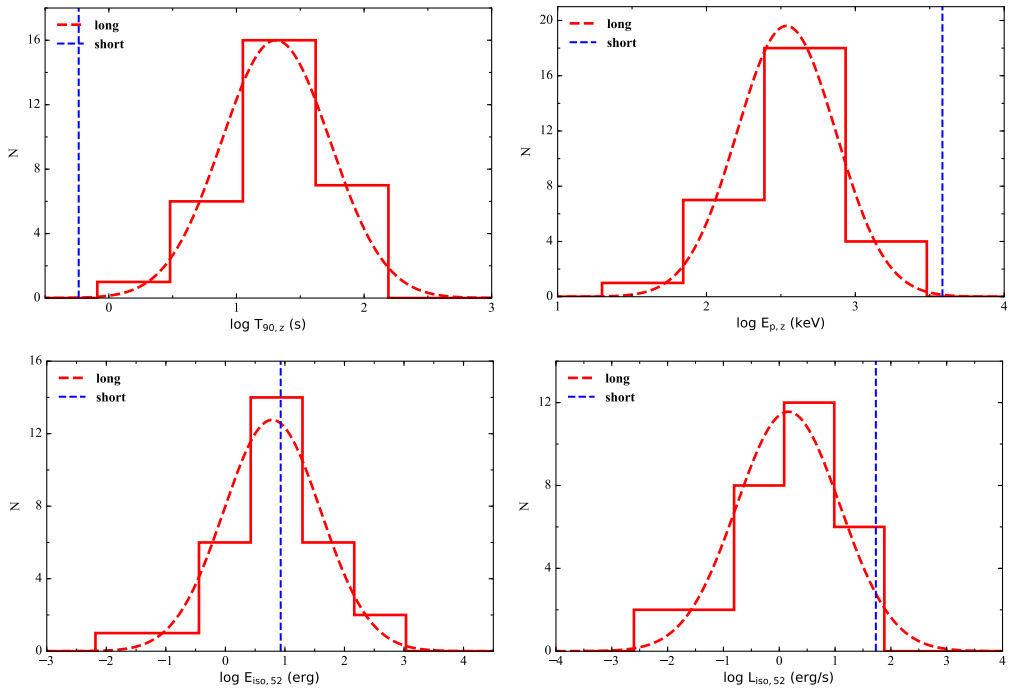

Figure 1. *Cont.*

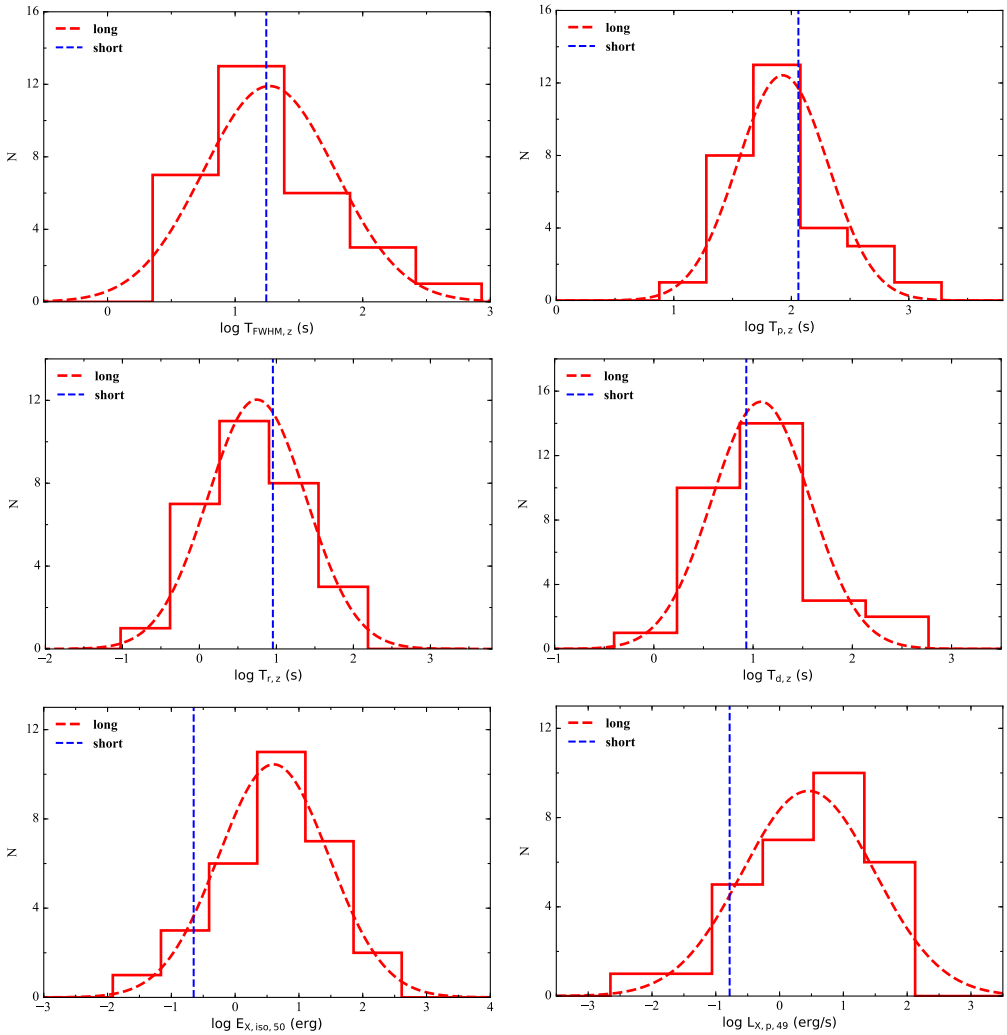

Figure 1. Distributions of prompt emissions and flares. The red soild and dashed lines represent the distributions and best-fit of LGRBs, respectively. The blue dashed lines represent the values of SGRBs.

3.2. Two-Parameter Correlations

It is generally believed that XRFs originate from the late activity of central engines. We wonder if there are some tight correlations between XRFs and prompt emission. The two-parameter correlations are analyzed and shown in Figure 2. We find that there really exist some tight correlations between the energy properties of prompt emission and XRFs, but almost no dependency in terms of time. We use the MCMC method to fit the correlations where the absolute value of the correlation coefficient is greater than 0.4. These correlations are shown in Figure 3, and the fit results are listed in Table 3.

The four very tight correlations are $E_{\rm iso} \propto E_{\rm X,iso}^{0.74\pm0.11}$ ($E_{\rm iso}$–$E_{\rm X,iso}$ correlation) with $r = 0.79$ and $\sigma_{\rm int} = 0.53$, $E_{\rm iso} \propto L_{\rm X,p}^{0.62\pm0.09}$ ($E_{\rm iso}$–$L_{\rm X,p}$ correlation) with $r = 0.79$ and $\sigma_{\rm int} = 0.53$, $L_{\rm iso} \propto E_{\rm X,iso}^{0.85\pm0.13}$ ($L_{\rm iso}$–$E_{\rm X,iso}$ correlation) with $r = 0.79$ and $\sigma_{\rm int} = 0.60$, and $L_{\rm iso} \propto L_{\rm X,p}^{0.68\pm0.11}$ ($L_{\rm iso}$–$L_{\rm X,p}$ correlation) with $r = 0.76$ and $\sigma_{\rm int} = 0.64$. From these correlations we find that the energy/luminosity of XRFs increases with the energy/luminosity increases of their prompt emission. This result is consistent with the previous studies [30,32], and strongly supports that prompt emission and XRFs may have a common central engine.

Furthermore, $E_{\rm p,z}$ has weak dependence on $E_{\rm X,iso}$ ($E_{\rm p,z} \propto E_{\rm X,iso}^{0.20\pm0.06}$ with $r = 0.52$), and $L_{\rm X,p}$ ($E_{\rm p,z} \propto L_{\rm X,p}^{0.16\pm0.05}$ with $r = 0.49$), respectively. However, $E_{\rm p,z}$ is independent form. the temporal parameters of XRFs. Interestingly, similar correlations between prompt

emission and the afterglow plateau phase have been revealed. Ref. [42] found that the luminosity corresponding to the end time (T_a) of the X-ray plateau phase ($L_{X,plateau}$) have tight correlations with E_{iso} and L_{iso} and have weak correlations with $E_{p,z}$. Ref. [43] found that the energy of the X-ray plateau phase ($E_{X,plateau}$) has correlations with E_{iso} and L_{iso}. Ref. [32] also found that the X-ray plateau phase and XRFs have similar correlations with prompt emission, respectively. These results may indicate that the physical origin of XRFs is likely to be the same as the plateau phase and they may originate from an energy-injection [32]. Meanwhile, we find no correlations between both the temporal and energy parameters of prompt emission and the temporal parameters of XRFs. The durations of prompt emission are independent from the duration, rise time, peak time, and decay times of the flares, which indicate that XRFs and prompt emission may come from different physical processes.

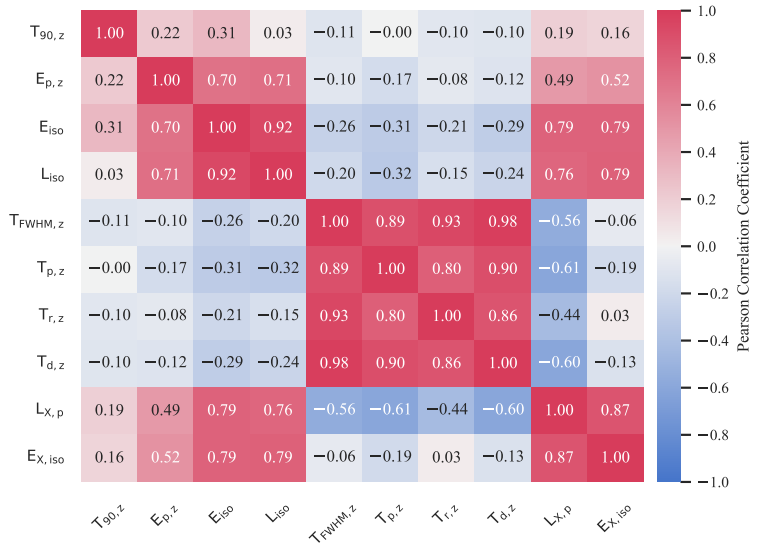

Figure 2. The. Pearson correlation coefficient matrix of the various parameters in the rest frame, where red and blue colors represent tight positive correlations and negative correlations, respectively.

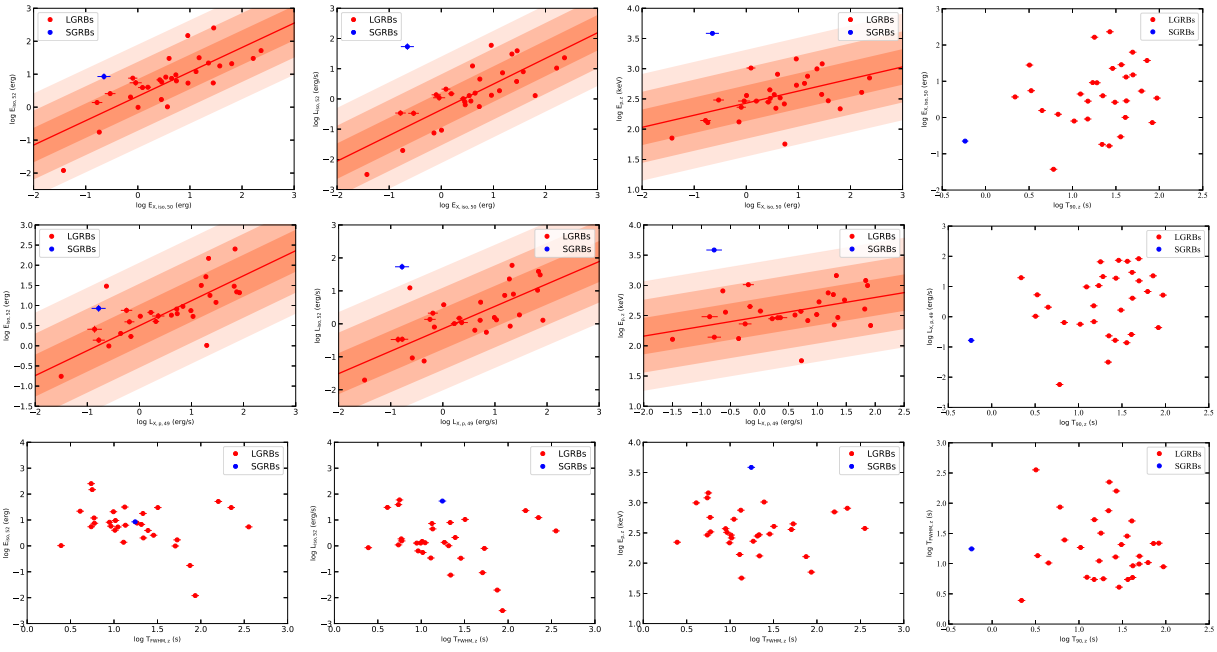

Figure 3. *Cont.*

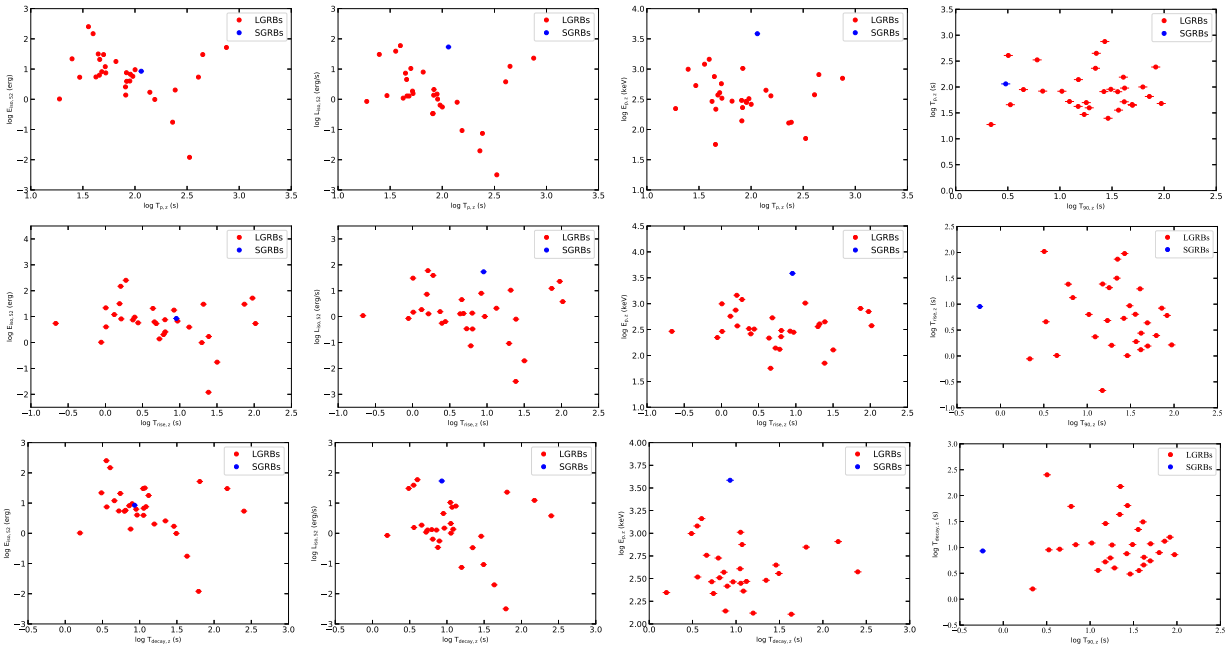

Figure 3. The two-parameter correlations between prompt emission and XRFs. The red and blue points present the LGRBs and SGRBs, respectively. The red shadows from dark to light represent the prediction interval of 1σ, 2σ and 3σ, respectively. The red lines are the best-fit lines.

Table 3. The results of the regression analysis of the correlations between XRFs and prompt emission, in which r is the Pearson correlation coefficient, and $\sigma_{\rm int}$ is the intrinsic scatter.

Relation	Expression	$\sigma_{\rm int}$	r
$E_{\rm iso}(E_{\rm X,iso})$	$\log E_{\rm iso,52} = (0.33 \pm 0.12) + (0.74 \pm 0.11) \times \log E_{\rm X,iso,50}$	0.53	0.79
$E_{\rm iso}(L_{\rm X,p})$	$\log E_{\rm iso,52} = (0.50 \pm 0.11) + (0.62 \pm 0.09) \times \log L_{\rm X,p,49}$	0.53	0.79
$L_{\rm iso}(E_{\rm X,iso})$	$\log L_{\rm iso,52} = (-0.36 \pm 0.13) + (0.85 \pm 0.13) \times \log E_{\rm X,iso,50}$	0.60	0.79
$L_{\rm iso}(L_{\rm X,p})$	$\log L_{\rm iso,52} = (-0.15 \pm 0.13) + (0.68 \pm 0.11) \times \log L_{\rm X,p,49}$	0.64	0.76
$E_{\rm p,z}(E_{\rm X,iso})$	$\log E_{\rm p,z} = (2.43 \pm 0.06) + (0.20 \pm 0.06) \times \log E_{\rm X,iso,50}$	0.25	0.52
$E_{\rm p,z}(L_{\rm X,p})$	$\log E_{\rm p,z} = (2.48 \pm 0.06) + (0.16 \pm 0.05) \times \log L_{\rm X,p,49}$	0.26	0.49

3.3. Three-Parameter Correlations

In general, the three-parameter relations can better constrain the physical model of GRBs. It is known that several tight three-parameter correlations between the X-ray plateau phase and the prompt emission of GRBs have found. Ref. [38] obtained $L_{\rm X,plateau} \propto T_{\rm a}^{-0.87} E_{\rm iso}^{0.88}$, which is confirmed by Ref. [39] ($L_{\rm X,plateau} \propto T_{\rm a}^{-1.01} E_{\rm iso}^{0.84}$) and Ref. [44] ($L_{\rm X,plateau} \propto T_{\rm a}^{-0.99} E_{\rm iso}^{0.86}$). A similar $L_{\rm X,plateau}$–$T_{\rm a}$–$L_{\rm iso}$ correlation was found by Ref. [45]. Furthermore, the $L_{\rm opt,plateau}$–$T_{\rm opt,a}$–$E_{\rm iso}$ correlation is also found in the optical afterglow, $L_{\rm opt,plateau} \propto T_{\rm opt,a}^{-0.9} E_{\rm iso}^{0.4}$, where $T_{\rm opt,a}$ is the end time of the optical plateau phase and $L_{\rm opt,plateau}$ is the corresponding luminosity [46].

Meanwhile, we explore the three-parameter correlations between XRFs and prompt emission. These correlations are shown in Figure 4, and the results of the regression analysis are listed in Table 4. The tight three-parameter sets are $\{E_{\rm iso}/L_{\rm iso}, E_{\rm X,iso}/L_{\rm X,p}, T_{\rm p,z}\}$, $\{E_{\rm iso}/L_{\rm iso}, E_{\rm p,z}, E_{\rm X,iso}/L_{\rm X,p}\}$, $\{E_{\rm X,iso}/L_{\rm X,p}, T_{\rm p,z}, E_{\rm p,z}\}$, and $\{E_{\rm X,iso}, E_{\rm p,z}, L_{\rm X,p}\}$. The tightest correlation is the $L_{\rm X,p}$–$T_{\rm p,z}$–$E_{\rm iso}$ correlation, which is expressed as $L_{\rm X,p} \propto T_{\rm p,z}^{-1.08} E_{\rm iso}^{0.84}$ with $r = 0.87$. We find that after accounting for the peak time of XRFs, the $L_{\rm X,p}$–$T_{\rm p,z}$–$E_{\rm iso}$ correlation is tighter than the $L_{\rm X,p}$–$E_{\rm iso}$ correlation. This may be due to $L_{\rm X,p}$ strongly depending on $T_{\rm p,z}$, which has been found in previous studies [12,13]. We also find that the $L_{\rm X,p}$–$T_{\rm p,z}$–$L_{\rm iso}$ correlation is tight, $L_{\rm X,p} \propto T_{\rm p,z}^{-1.09} L_{\rm iso}^{0.71}$ with $r = 0.85$. Interestingly, the three-parameter correlations of GRBs associated with XRFs are similar to those of the

plateau phase, which further supports that XRFs have a common origin with the plateau phase.

In addition, when $E_{\rm X,iso}$ is used instead of $L_{\rm X,p}$, the $E_{\rm X,iso}$–$T_{\rm p,z}$–$E_{\rm iso}$ ($E_{\rm X,iso} \propto T_{\rm p,z}^{0.12} E_{\rm iso}^{0.85}$, $r = 0.79$) and $E_{\rm X,iso}$–$T_{\rm p,z}$–$L_{\rm iso}$ ($E_{\rm X,iso} \propto T_{\rm p,z}^{0.15} L_{\rm iso}^{0.76}$, $r = 0.79$) correlations are still tight. However, the coefficient of $T_{\rm p,z}$ in the $E_{\rm X,iso}$–$T_{\rm p,z}$–$E_{\rm iso}/L_{\rm iso}$ correlation is significantly lower than that of the other parameter, which may be caused by the weak correlation between $E_{\rm X,iso}$ and $T_{\rm p,z}$. Interestingly, after swapping $E_{\rm X,iso}$ and $E_{\rm iso}/L_{\rm iso}$, the correlations become tighter, $E_{\rm iso} \propto T_{\rm p,z}^{-0.35} E_{\rm X,iso}^{0.71}$, $r = 0.80$, and $L_{\rm iso} \propto T_{\rm p,z}^{-0.42} E_{\rm X,iso}^{0.81}$, $r = 0.81$, respectively. More importantly, the coefficient between $T_{\rm p,z}$ and the other parameter is not significantly different, and the $E_{\rm iso}/L_{\rm iso}$–$T_{\rm p,z}$–$E_{\rm X,iso}$ correlations are jointly contributed by both $T_{\rm p,z}$ and $E_{\rm X,iso}$.

We also study three-parameter correlations involving $E_{\rm p,z}$. After accounting for $T_{\rm p,z}$, $E_{\rm p,z}$ also has weak correlations with $E_{\rm X,iso}$, $E_{\rm X,iso} \propto T_{\rm p,z}^{-0.21} E_{\rm p,z}^{1.41}$, and $L_{\rm X,p}$, $L_{\rm X,p} \propto T_{\rm p,z}^{-1.43} E_{\rm p,z}^{1.28}$, respectively. Similarly, the $E_{\rm X,plateau}$–$T_{\rm a,z}$–$E_{\rm p,z}$ correlation and the $L_{\rm opt,plateau}$–$T_{\rm a,z}$–$E_{\rm p,z}$ correlation were also found in the X-ray and optical afterglow, respectively [43,46].

Table 4. The results of the regression analysis for three-parameter correlations, in which r is the Pearson correlation coefficient, and $\sigma_{\rm int}$ is the intrinsic scatter.

Relation	Expression	$\sigma_{\rm int}$	r
$\{L_{\rm X,p}, T_{\rm p,z}, E_{\rm iso}\}$	$\log L_{\rm X,p,49} = (1.88 \pm 0.57) + (-1.08 \pm 0.27) \times \log T_{\rm p,z} + (0.84 \pm 0.13) \times \log E_{\rm iso,52}$	0.54	0.87
	$\log E_{\rm iso,52} = (-0.64 \pm 0.63) + (0.56 \pm 0.31) \times \log T_{\rm p,z} + (0.75 \pm 0.11) \times \log L_{\rm X,p,49}$	0.51	0.81
	$\log T_{\rm p,z} = (1.93 \pm 0.08) + (-0.36 \pm 0.09) \times \log L_{\rm X,p,49} + (0.21 \pm 0.11) \times \log E_{\rm iso,52}$	0.31	0.66
$\{E_{\rm X,iso}, L_{\rm X,p}, E_{\rm p,z}\}$	$\log E_{\rm X,iso,50} = (-0.60 \pm 0.73) + (0.66 \pm 0.09) \times \log L_{\rm X,p,49} + (0.36 \pm 0.30) \times \log E_{\rm p,z}$	0.45	0.87
	$\log L_{\rm X,p,49} = (-0.55 \pm 0.89) + (1.01 \pm 0.14) \times \log E_{\rm X,iso,50} + (0.16 \pm 0.37) \times \log E_{\rm p,z}$	0.56	0.87
	$\log E_{\rm p,z} = (2.44 \pm 0.06) + (0.04 \pm 0.10) \times \log L_{\rm X,p,49} + (0.15 \pm 0.11) \times \log E_{\rm X,iso,50}$	0.26	0.53
$\{L_{\rm iso}, E_{\rm p,z}, E_{\rm X,iso}\}$	$\log L_{\rm iso,52} = (-4.27 \pm 0.91) + (1.61 \pm 0.35) \times \log E_{\rm p,z} + (0.52 \pm 0.12) \times \log E_{\rm X,iso,50}$	0.41	0.86
	$\log E_{\rm X,iso,50} = (1.13 \pm 1.24) + (-0.26 \pm 0.45) \times \log E_{\rm p,z} + (0.81 \pm 0.17) \times \log L_{\rm iso,52}$	0.56	0.79
	$\log E_{\rm p,z} = (2.54 \pm 0.05) + (0.31 \pm 0.06) \times \log L_{\rm iso,52} + (-0.06 \pm 0.06) \times \log E_{\rm X,iso,50}$	0.17	0.72
$\{E_{\rm iso}, E_{\rm p,z}, L_{\rm X,p}\}$	$\log E_{\rm iso,52} = (-2.37 \pm 0.80) + (1.16 \pm 0.32) \times \log E_{\rm p,z} + (0.43 \pm 0.09) \times \log L_{\rm X,p}$	0.41	0.86
	$\log L_{\rm X,p,49} = (0.51 \pm 1.26) + (-0.37 \pm 0.51) \times \log E_{\rm p,z} + (1.11 \pm 0.22) \times \log E_{\rm iso,52}$	0.68	0.79
	$\log E_{\rm p,z} = (2.31 \pm 0.06) + (0.33 \pm 0.08) \times \log E_{\rm iso,52} + (-0.04 \pm 0.06) \times \log L_{\rm X,p,49}$	0.20	0.71
$\{L_{\rm X,p}, T_{\rm p,z}, L_{\rm iso}\}$	$\log L_{\rm X,p,49} = (2.44 \pm 0.58) + (-1.09 \pm 0.29) \times \log T_{\rm p,z} + (0.71 \pm 0.12) \times \log L_{\rm iso,52}$	0.58	0.85
	$\log L_{\rm iso,52} = (-1.23 \pm 0.78) + (0.53 \pm 0.38) \times \log T_{\rm p,z} + (0.80 \pm 0.14) \times \log L_{\rm X,p,49}$	0.62	0.78
	$\log T_{\rm p,z} = (2.05 \pm 0.07) + (-0.32 \pm 0.09) \times \log L_{\rm X,p,49} + (0.14 \pm 0.10) \times \log L_{\rm iso,52}$	0.32	0.64
$\{E_{\rm iso}, E_{\rm p,z}, E_{\rm X,iso}\}$	$\log E_{\rm iso,52} = (-2.39 \pm 0.83) + (1.13 \pm 0.34) \times \log E_{\rm p,z} + (0.51 \pm 0.12) \times \log E_{\rm X,iso,50}$	0.43	0.85
	$\log E_{\rm X,iso,50} = (0.25 \pm 1.05) + (-0.13 \pm 0.45) \times \log E_{\rm p,z} + (0.87 \pm 0.18) \times \log E_{\rm iso,52}$	0.57	0.79
	$\log E_{\rm p,z} = (2.32 \pm 0.06) + (0.30 \pm 0.08) \times \log E_{\rm iso,52} + (-0.02 \pm 0.07) \times \log E_{\rm X,iso,50}$	0.20	0.70
$\{L_{\rm iso}, E_{\rm p,z}, L_{\rm X,p}\}$	$\log L_{\rm iso,52} = (-4.43 \pm 0.93) + (1.72 \pm 0.35) \times \log E_{\rm p,z} + (0.40 \pm 0.10) \times \log L_{\rm X,p,49}$	0.43	0.85
	$\log L_{\rm X,p,49} = (1.28 \pm 1.58) + (-0.39 \pm 0.58) \times \log E_{\rm p,z} + (0.95 \pm 0.22) \times \log L_{\rm iso,52}$	0.72	0.77
	$\log E_{\rm p,z} = (2.53 \pm 0.04) + (0.31 \pm 0.05) \times \log L_{\rm iso,52} + (-0.05 \pm 0.05) \times \log L_{\rm X,p,49}$	0.16	0.72
$\{L_{\rm iso}, T_{\rm p,z}, E_{\rm X,iso}\}$	$\log L_{\rm iso,52} = (0.48 \pm 0.58) + (-0.42 \pm 0.28) \times \log T_{\rm p,z} + (0.81 \pm 0.13) \times \log E_{\rm X,iso,50}$	0.58	0.81
	$\log E_{\rm X,iso,50} = (0.19 \pm 0.56) + (0.15 \pm 0.29) \times \log T_{\rm p,z} + (0.76 \pm 0.12) \times \log L_{\rm iso,52}$	0.56	0.79
	$\log T_{\rm p,z} = (1.91 \pm 0.10) + (0.08 \pm 0.14) \times \log E_{\rm X,iso,50} + (-0.19 \pm 0.13) \times \log L_{\rm iso,52}$	0.39	0.34
$\{E_{\rm iso}, T_{\rm p,z}, E_{\rm X,iso}\}$	$\log E_{\rm iso,52} = (1.02 \pm 0.52) + (-0.35 \pm 0.25) \times \log T_{\rm p,z} + (0.71 \pm 0.11) \times \log E_{\rm X,iso,50}$	0.52	0.80
	$\log E_{\rm X,iso,50} = (-0.30 \pm 0.60) + (0.12 \pm 0.29) \times \log T_{\rm p,z} + (0.85 \pm 0.14) \times \log E_{\rm iso,52}$	0.57	0.79
	$\log T_{\rm p,z} = (2.05 \pm 0.10) + (0.06 \pm 0.14) \times \log E_{\rm X,iso,50} + (-0.20 \pm 0.14) \times \log E_{\rm iso,52}$	0.40	0.32
$\{T_{\rm p,z}, L_{\rm X,p}, E_{\rm p,z}\}$	$\log T_{\rm p,z} = (1.58 \pm 0.51) + (-0.25 \pm 0.07) \times \log L_{\rm X,p,49} + (0.18 \pm 0.21) \times \log E_{\rm p,z}$	0.33	0.62
	$\log E_{\rm p,z} = (2.19 \pm 0.34) + (0.14 \pm 0.17) \times \log T_{\rm p,z} + (0.19 \pm 0.06) \times \log L_{\rm X,p,49}$	0.27	0.51
	$\log L_{\rm X,p,49} = (-0.05 \pm 1.51) + (-1.43 \pm 0.38) \times \log T_{\rm p,z} + (1.28 \pm 0.47) \times \log E_{\rm p,z}$	0.77	0.51
$\{E_{\rm p,z}, T_{\rm p,z}, E_{\rm X,iso}\}$	$\log E_{\rm p,z} = (2.59 \pm 0.27) + (-0.08 \pm 0.13) \times \log T_{\rm p,z} + (0.19 \pm 0.06) \times \log E_{\rm X,iso,50}$	0.26	0.53
	$\log E_{\rm X,iso,50} = (-2.59 \pm 1.56) + (-0.21 \pm 0.38) \times \log T_{\rm p,z} + (1.41 \pm 0.49) \times \log E_{\rm p,z}$	0.78	0.53
	$\log T_{\rm p,z} = (2.27 \pm 0.67) + (-0.06 \pm 0.10) \times \log E_{\rm X,iso,50} + (-0.12 \pm 0.26) \times \log E_{\rm p,z}$	0.41	0.21

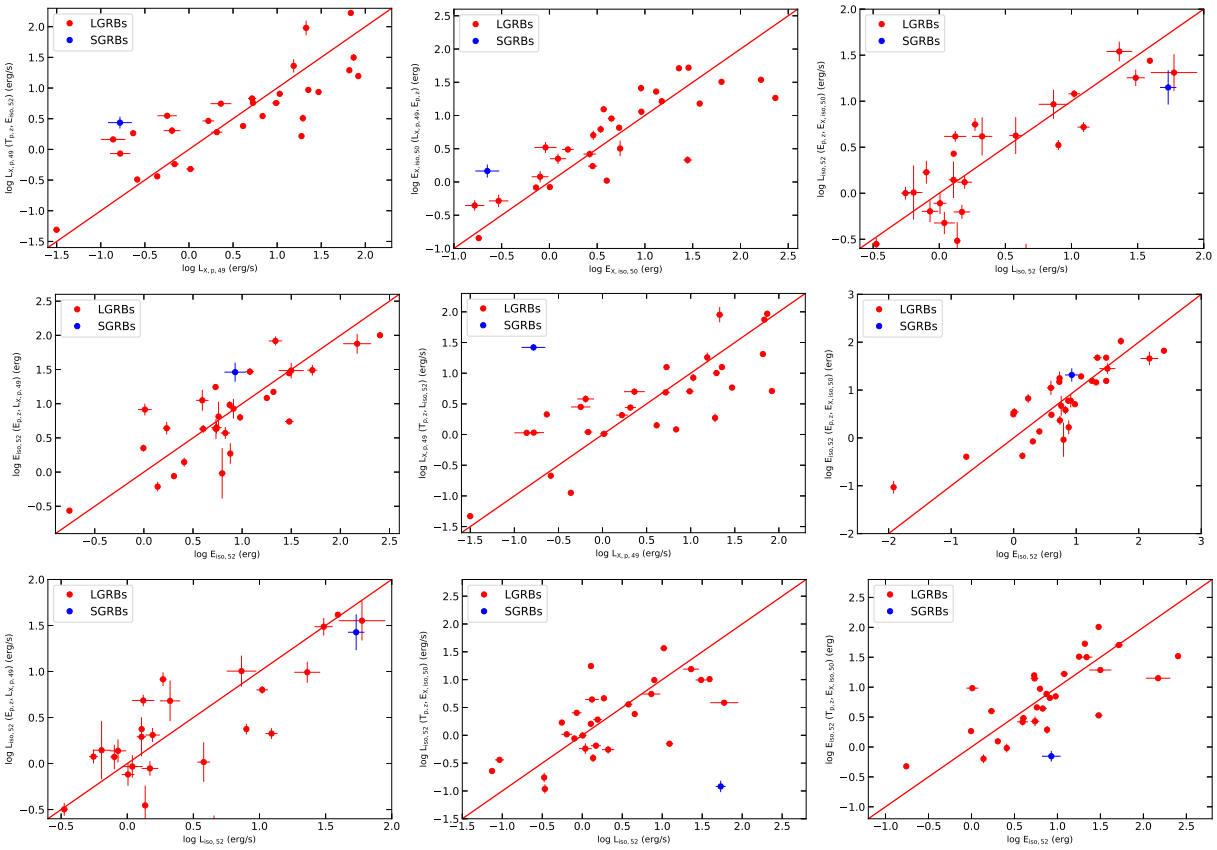

Figure 4. The three-parameter correlations between prompt emission and XRFs. The red and blue points present the LGRBs and SGRBs, respectively. The red lines represent y = x.

4. Summary

In this work, we compile a GRB sample containing 31 GRBs with single XRFs, that are well-constrained $E_{\rm p}$, and redshifts, and analyze the properties and correlations between prompt emission and XRFs in the rest frame. We find that the prompt emission and XRF parameters of GRBs are basically log-normal distributions. The meadian value of the flare rise time is shorter than the flare decay time, with a ratio of about 1:2, which is similar to the FRED structure of prompt emission pulses [41].

We explore the two-parameter correlations between prompt emission and XRFs. We find there are several tight correlations between $E_{\rm iso}/L_{\rm iso}$ and $E_{\rm X,iso}/L_{\rm X,p}$. Such as $E_{\rm iso} \propto E_{\rm X,iso}^{0.74}$ ($L_{\rm X,p}^{0.62}$) with $r = 0.79$ (0.79) and $L_{\rm iso} \propto E_{\rm X,iso}^{0.85}$ ($L_{\rm X,p}^{0.68}$) with $r = 0.79$ (0.76). This indicates that the flare energy/luminosity strongly depend on the prompt emission energy/luminosity. The prompt emission peak energy and the flare energy/luminosity are weakly dependent, $E_{\rm p,z} \propto E_{\rm X,iso}^{0.20}$ with $r = 0.52$, and $E_{\rm p,z} \propto L_{\rm X,p}^{0.16}$ with $r = 0.49$, respectively. These results suggest that the prompt emission and XRFs may originate from the common central engine. Meanwhile, we find that the temporal and energy parameters of the prompt emission and the temporal parameters of XRFs are independent.

In addition, the three-parameter correlations between the prompt emission and XRFs are also analyzed. We find several tight three-parameter correlations, such as $L_{\rm X,p} \propto T_{\rm p,z}^{-1.08} E_{\rm iso}^{0.84}$ with $r = 0.87$ and $L_{\rm X,p} \propto T_{\rm p,z}^{-1.09} L_{\rm iso}^{0.71}$ with $r = 0.85$. Interestingly, the $L_{\rm X,p}$–$T_{\rm p,z}$–$E_{\rm iso}$ correlation is similar to the $L_{\rm X,plateau}$–$T_{\rm a}$–$E_{\rm iso}$ correlation of the X-ray plateau phase [38,39,44] and the $L_{\rm opt,plateau}$–$T_{\rm opt,a}$–$E_{\rm iso}$ correlation of the optical plateau phase [46]. The $L_{\rm X,p}$–$T_{\rm p,z}$–$L_{\rm iso}$ correlation is also similar to the $L_{\rm X,plateau}$–$T_{\rm a}$–$L_{\rm iso}$ correlation of the X-ray plateau [45]. Furthermore, the $E_{\rm X,iso}/L_{\rm X,p}$–$T_{\rm p,z}$–$E_{\rm p,z}$ correlations are also confirmed [43,46]. These indicate that the flares and the plateau phase may have the same physical origin. However, the occurrence time and characteristics of the flares and the plateau phase are

different, and it is more likely that they are in a different phase of the same physical process [32]. Generally, the plateau phase is considered to be the energy injections from the spin-down of a millisecond magnetar, which implicates that XRFs may be driven by magnetar activity. Due to the small sample size, the results obtained above need to be improved through more observations. The Space-based multi-band Variable Object Monitor (SVOM) and Einstein Probe (EP) are expected to observe more GRBs with XRFs, redshifts, and a well-constrained spectrum.

Author Contributions: X.-T.Z., S.-Y.Z. and F.-W.Z. led the data analysis and wrote the manuscript. L.-M.Z. and Z.Z. helped with the data analysis. All authors have read and agreed to the published version of the manuscript.

Funding: This research was funded in part by the Guangxi Natural Science Foundation (No. 2022GXNSFDA035083) and by the National Natural Science Foundation of China (No. 11763003).

Data Availability Statement: The Fermi GRB data underlying this article are publicly available within the Fermi Catalog, accessed on 1 June 2020, https://heasarc.gsfc.nasa.gov/W3Browse/fermi/fermigbrst.html.

Acknowledgments: We thank the anonymous reviewers for their insightful comments/suggestions.

Conflicts of Interest: The authors declare no conflicts of interest.

Notes

[1] https://heasarc.gsfc.nasa.gov/W3Browse/fermi/fermigbrst.html, accessed on 1 May 2024.
[2] https://gcn.nasa.gov/, accessed on 1 May 2024.
[3] https://pypi.python.org/pypi/emcee, accessed on 1 May 2024.

References

1. Kouveliotou, C.; Meegan, C.A.; Fishman, G.J.; Bhat, N.P.; Briggs, M.S.; Koshut, T.M.; Paciesas, W.S.; Pendleton, G.N. Identification of Two Classes of Gamma-Ray Bursts. *Astrophys. J. Lett.* **1993**, *413*, L101. [CrossRef]
2. Paczynski, B. Gamma-ray bursters at cosmological distances. *Astrophys. J. Lett.* **1986**, *308*, L43. [CrossRef]
3. Kochanek, C.S.; Piran, T. Gravitational Waves and gamma-Ray Bursts. *Astrophys. J. Lett.* **1993**, *417*, L17. [CrossRef]
4. Woosley, S.E. Gamma-Ray Bursts from Stellar Mass Accretion Disks around Black Holes. *Astrophys. J.* **1993**, *405*, 273. [CrossRef]
5. Kumar, P.; Zhang, B. The physics of gamma-ray bursts & relativistic jets. *Phys. Rep.* **2015**, *561*, 1. [CrossRef]
6. Gehrels, N.; Chincarini, G.; Giommi, P.; Mason, K.O.; Nousek, J.A.; Wells, A.A.; White, N.E.; Barthelmy, S.D.; Burrows, D.N.; Cominsky, L.R.; et al. The Swift Gamma-Ray Burst Mission. *Astrophys. J.* **2004**, *611*, 1005. [CrossRef]
7. Zhang, B.; Fan, Y.Z.; Dyks, J.; Kobayashi, S.; Mészáros, P.; Burrows, D.N.; Nousek, J.A.; Gehrels, N. Physical Processes Shaping Gamma-Ray Burst X-ray Afterglow Light Curves: Theoretical Implications from the Swift X-ray Telescope Observations. *Astrophys. J.* **2006**, *642*, 354. [CrossRef]
8. Campana, S.; Tagliaferri, G.; Lazzati, D.; Chincarini, G.; Covino, S.; Page, K.; Romano, P.; Moretti, A.; Cusumano, G.; Mangano, V.; et al. The X-ray Afterglow of the Short Gamma Ray Burst 050724. *Astron. Astrophys.* **2006**, *454*, 113. [CrossRef]
9. Falcone, A.D.; Burrows, D.N.; Lazzati, D.; Campana, S.; Kobayashi, S.; Zhang, B.; Mészáros, P.; Page, K.L.; Kennea, J.A.; Romano, P.; et al. The Giant X-ray Flare of GRB 050502B: Evidence for Late-Time Internal Engine Activity. *Astrophys. J.* **2006**, *641*, 1010. [CrossRef]
10. Nousek, J.A.; Kouveliotou, C.; Grupe, D.; Page, K.L.; Granot, J.; Ramirez-Ruiz, E.; Patel, S.K.; Burrows D.N.; Mangano, V.; Barthelmy, S.; et al. Evidence for a Canonical Gamma-Ray Burst Afterglow Light Curve in the Swift XRT Data. *Astrophys. J.* **2006**, *642*, 389. [CrossRef]
11. Margutti, R.; Chincarini, G.; Granot, J.; Guidorzi, C.; Berger, E.; Bernardini, M.G.; Gehrels, N.; Soderberg, A.M.; Stamatikos, M.; Zaninoni, E. X-ray Flare Candidates in Short Gamma-Ray Bursts. *Mon. Not. R. Astron. Soc.* **2011**, *417*, 2144. [CrossRef]
12. Yi, S.-X.; Xi, S.-Q.; Yu, H.; Wang, F.Y.; Mu, H.-J.; Lü, L.Z.; Liang, E.-W. Comprehensive Study of the X-ray Flares from Gamma-Ray Bursts Observed by Swift. *Astrophys. J. Suppl. Ser.* **2016**, *224*, 20. [CrossRef]
13. Shi, Y.-R.; Ding, X.-K.; Zhu, S.-Y.; Sun, W.-P.; Zhang, F.-W. Statistical Properties of X-ray Flares in Gamma-Ray Bursts. *Universe* **2022**, *8*, 358. [CrossRef]
14. Curran, P.A.; Starling, R.L.C.; O'Brien, P.T.; Godet, O.; van der Horst, A.J.; Wijers, R.A.M.J. On the nature of late X-ray flares in Swift gamma-ray bursts. *Astron. Astrophys.* **2008**, *487*, 533. [CrossRef]
15. Bernardini, M.G.; Margutti, R.; Chincarini, G.; Guidorzi, C.; Mao, J. Gamma-Ray Burst Long Lasting X-ray Flaring Activity. *Astron. Astrophys.* **2011**, *526*, A27. [CrossRef]
16. Mészáros, P.; Rees, M.J. Optical and Long-Wavelength Afterglow from Gamma-Ray Bursts. *Astrophys. J.* **1997**, *476*, 232. [CrossRef]

17. Kobayashi, S.; Zhang, B.; Mészáros, P.; Burrows, D. Inverse Compton X-ray Flare from Gamma-Ray Burst Reverse Shock. *Astrophys. J.* **2007**, *655*, 391. [CrossRef]
18. Chincarini, G.; Moretti, A.; Romano, P.; Falcone, A.D.; Morris, D.; Racusin, J.; Campana, S.; Covino, S.; Guidorzi, C.; Tagliaferri, G.; et al. The First Survey of X-ray Flares from Gamma-Ray Bursts Observed by Swift: Temporal Properties and Morphology. *Astrophys. J.* **2007**, *671*, 1903. [CrossRef]
19. Rees, M.J.; Mészáros, P. Refreshed Shocks and Afterglow Longevity in Gamma-Ray Bursts. *Astrophys. J. Lett.* **1998**, *496*, L1. [CrossRef]
20. Ioka, K.; Kobayashi, S.; Zhang, B. Variabilities of Gamma-Ray Burst Afterglows: Long-acting Engine, Anisotropic Jet, or Many Fluctuating Regions? *Astrophys. J.* **2005**, *631*, 429. [CrossRef]
21. Zhang, B.; Mészáros, P. Gamma-Ray Bursts with Continuous Energy Injection and Their Afterglow Signature. *Astrophys. J.* **2002**, *566*, 712. [CrossRef]
22. Burrows, D.N.; Romano, P.; Falcone, A.; Kobayashi, S.; Zhang, B.; Moretti, A.; O'Brien, P.T.; Goad, M.R.; Campana, S.; Page, K.L.; et al. Bright X-ray Flares in Gamma-Ray Burst Afterglows. *Science* **2005**, *309*, 1833. [CrossRef] [PubMed]
23. Chincarini, G.; Mao, J.; Margutti, R.; Bernardini, M.G.; Guidorzi, C.; Pasotti, F.; Giannios, D.; Della Valle, M.; Moretti, A.; Romano, P.; et al. Unveiling the Origin of X-ray Flares in Gamma-Ray Bursts. *Mon. Not. R. Astron. Soc.* **2010**, *406*, 2113. [CrossRef]
24. Falcone, A.D.; Morris, D.; Racusin, J.; Chincarini, G.; Moretti, A.; Romano, P.; Burrows, D.N.; Pagani, C.; Stroh, M.; Grupe, D.; et al. The First Survey of X-ray Flares from Gamma-Ray Bursts Observed by Swift: Spectral Properties and Energetics. *Astrophys. J.* **2007**, *671*, 1921. [CrossRef]
25. Lü, L.-Z.; Liang, E.-W.; Cordier, B. The Spectral Evolution Patterns and Implications of Gamma-Ray Burst X-ray Flares. *Astrophys. J.* **2022**, *941*, 99. [CrossRef]
26. Margutti, R.; Guidorzi, C.; Chincarini, G.; Bernardini, M.G.; Genet, F.; Mao, J.; Pasotti, F. Lag-luminosity relation in gamma-ray burst X-ray flares: A direct link to the prompt emission. *Mon. Not. R. Astron. Soc.* **2010**, *406*, 2149. [CrossRef]
27. Sonbas, E.; MacLachlan, G.A.; Shenoy, A.; Dhuga, K.S.; Parke, W.C. A New Correlation between GRB X-ray Flares and the Prompt Emission. *Astrophys. J. Lett.* **2013**, *767*, L28. [CrossRef]
28. Chang, X.Z.; Peng, Z.Y.; Chen, J.M.; Yin, Y.; Wang, D.Z.; Wu, H. A Comprehensive Study of Multiflare GRB Spectral Lag. *Astrophys. J.* **2021**, *922*, 34. [CrossRef]
29. Peng, F.-K.; Liang, E.-W.; Wang, X.-Y.; Hou, S.-J.; Xi, S.-Q.; Lu, R.-J.; Zhang, J.; Zhang, B. Photosphere Emission in the X-ray Flares of Swift Gamma-Ray Bursts and Implications for the Fireball Properties. *Astrophys. J.* **2014**, *795*, 155. [CrossRef]
30. Wang, Y.; Aimuratov, Y.; Moradi, R.; Peresano, M.; Ruffini, R.; Shakeri, S. Revisiting the Statistics of X-ray Flares in Gamma-Ray Bursts. *Mem. Soc. Astron. Ital.* **2018**, *89*, 293. [CrossRef]
31. Yi, S.-X.; Xie, W.; Ma, S.-B.; Lei, W.-H.; Du, M. Constraining Properties of GRB Central Engines with X-ray Flares. *Mon. Not. R. Astron. Soc.* **2021**, *507*, 1047. [CrossRef]
32. Yi, S.-X.; Du, M.; Liu, T. Statistical Analyses of the Energies of X-ray Plateaus and Flares in Gamma-Ray Bursts. *Astrophys. J.* **2022**, *924*, 69. [CrossRef]
33. Saji, J.; Iyyani, S.; Mazde, K. Statistical Analysis of Long GRBs' Prompt Emission and X-ray Flares: Multivariate Clustering and Correlations. *Astrophys. J. Suppl. Ser.* **2023**, *269*, 2. [CrossRef]
34. Wang, F.Y.; Dai, Z.G. Self-organized Criticality in X-ray Flares of Gamma-Ray-Burst Afterglows. *Nat. Phys.* **2013**, *9*, 465. [CrossRef]
35. Schaefer, B.E. The Hubble Diagram to Redshift >6 from 69 Gamma-Ray Bursts. *Astrophys. J.* **2007**, *660*, 16. [CrossRef]
36. Band, D.; Matteson, J.; Ford, L.; Schaefer, B.; Palmer, D.; Teegarden, B.; Cline, T.; Briggs, M.; Paciesas, W.; Pendleton, G.; et al. BATSE Observations of Gamma-Ray Burst Spectra. I. Spectral Diversity. *Astrophys. J.* **1993**, *413*, 281. [CrossRef]
37. D'Agostini, G. Fits, and especially linear fits, with errors on both axes, extra variance of the data points and other complications. *arXiv* **2005**, arXiv:physics/0511182.
38. Xu, M.; Huang, Y.F. New three-parameter correlation for gamma-ray bursts with a plateau phase in the afterglow. *Astron. Astrophys.* **2012**, *538*, A134. [CrossRef]
39. Tang, C.-H.; Huang, Y.-F.; Geng, J.-J.; Zhang, Z.-B. Statistical Study of Gamma-Ray Bursts with a Plateau Phase in the X-ray Afterglow. *Astrophys. J. Suppl. Ser.* **2019**, *245*, 1. [CrossRef]
40. Foreman-Mackey, D.; Hogg, D.W.; Lang, D.; Goodman, J. emcee: The MCMC Hammer. *Publ. Astron. Soc. Pac.* **2013**, *125*, 306. [CrossRef]
41. Norris, J.P.; Nemiroff, R.J.; Bonnell, J.T.; Scargle, J.D.; Kouveliotou, C.; Paciesas, W.S.; Meegan, C.A.; Fishman, G.J. Attributes of Pulses in Long Bright Gamma-Ray Bursts. *Astrophys. J.* **1996**, *459*, 393. [CrossRef]
42. Dainotti, M.G.; Ostrowski, M.; Willingale, R. Towards a standard gamma-ray burst: Tight correlations between the prompt and the afterglow plateau phase emission. *Mon. Not. R. Astron. Soc.* **2011**, *418*, 2202. [CrossRef]
43. Ding, X.-K.; Shi, Y.-R.; Zhu, S.-Y.; Sun, W.-P.; Zhang, F.-W. Statistical properties of the X-ray afterglow shallow decay phase and their relationships with the prompt gamma-ray emission of gamma-ray bursts. *Astrophys. Space Sci.* **2022**, *367*, 58. [CrossRef]
44. Deng, C.; Huang, Y.-F.; Xu, F. Pseudo-redshifts of Gamma-Ray Bursts Derived from the L-T-E Correlation. *Astrophys. J.* **2023**, *943*, 126. [CrossRef]

45. Dainotti, M.G.; Postnikov, S.; Hernandez, X.; Ostrowski, M. A Fundamental Plane for Long Gamma-Ray Bursts with X-ray Plateaus. *Astrophys. J. Lett.* **2016**, *825*, L20. [CrossRef]
46. Si, S.-K.; Qi, Y.-Q.; Xue, F.-X.; Liu, Y.-J.; Wu, X.; Yi, S.-X.; Tang, Q.-W.; Zou, Y.-C.; Wang, F.-F.; Wang, X.-G. The Three-parameter Correlations About the Optical Plateaus of Gamma-Ray Bursts. *Astrophys. J.* **2018**, *863*, 50. [CrossRef]